Propagation of action potentials along complex axonal trees
Model and implementation

Yair Manor*, Jacob Gonczarowski‡, and Idan Segev
Department of Neurobiology, Institute of Life Sciences*; and Department of Computer Sciences,‡ Hebrew University, Jerusalem, 91904, Israel

ABSTRACT Axonal trees are typically morphologically and physiologically complicated structures. Because of this complexity, axonal trees show a large repertoire of behavior: from transmission lines with delay, to frequency filtering devices in both temporal and spatial domains.

Detailed theoretical exploration of the electrical behavior of realistically complex axonal trees is notably lacking, mainly because of the absence of a simple modeling tool. AXONTREE is an attempt to provide such a simulator. It is written in C for the SUN workstation and implements both a detailed compartmental modeling of Hodgkin and Huxley-like kinetics, and a more abstract, event-driven, modeling approach. The computing module of AXONTREE is introduced together with its input/output features. These features allow graphical construction of arbitrary trees directly on the computer screen, and superimposition of the results on the simulated structure. Several numerical improvements that increase the computational efficiency by a factor of 5–10 are presented; most notable is a novel method of dynamic lumping of the modeled tree into simpler representations ("equivalent cables"). AXONTREE's performance is examined using a reconstructed terminal of an axon from a Y cell in cat visual cortex. It is demonstrated that realistically complicated axonal trees can be handled efficiently. The application of AXONTREE for the study of propagation delays along axonal trees is presented in the companion paper (Manor et al., 1991).

INTRODUCTION

Axons are classically considered as being merely faithful transmission lines. According to this view, when threshold conditions for firing an action potential (AP) at the axon hillock are achieved, a digital ("all-or-none") signal is produced and propagates fast and securely (with a high safety factor) to all output sites of the axonal tree. Because the propagation velocity is rather high, the AP is thought to arrive almost simultaneously to all these sites (which may reach several thousands in a single axon. See for example, Kisvarday et al., 1987; Sereno and Ulinski, 1987).

Nonetheless, a large body of experimental findings suggest that these classical concepts should be reexamined. It was experimentally demonstrated that short bursts of APs show intermittent failure at certain regions along the axon (e.g., Barron and Matthews, 1935; Bittner, 1968; Raymond and Lettvin, 1969; Parnas, 1972; Chung et al., 1970; Grossman et al., 1979). These studies have also shown that APs may be routed differentially into daughter branches of the same axon and that this filtering depends on the frequency of the APs. Several studies have also suggested that certain axons function as asynchronous rather than synchronous elements (Braitenberg, 1967; Freeman, 1969; Carr and Konishi, 1988). These and other studies indicate that axons may play a role in the processing of neuronal information (see reviews by Waxman, 1975; Parnas, 1979; Swadlow et al., 1980).

Although the name axon (axis in Greek) implies a rather homogeneous, long structure, axons show regional specialization in both their electrical and morphological properties. For example, the axon hillock contains a particularly high density of excitable (Na^+) channels (Hille, 1984), whereas near the synaptic release sites, voltage-gated Ca^{2+} channels are concentrated. Morphologically, axons usually bifurcate several times, send collaterals and often create large trees. At their terminal arborizations, axons of both vertebrate and invertebrate typically have multiple successive diameter changes, from a thin (sometimes 0.1 μm) bottleneck to a thick (0.5–3 μm) varicosity, or boutons (for an impressive example, see the work of Sereno and Ulinski, 1987; see also recent studies on the distribution of boutons in cortical cells by Schüz and Münster, 1985; Kisvarday et al., 1987; Rockland, 1989). Electron micrograph studies show that in most cases the varicose region contains synaptic vesicles, indicating that the boutons are the major output sites of the neuron (Jahromi and Atwood, 1974; Fyffe and Light, 1984; Schüz and Münster, 1985).

Theoretical studies that are based on experimental data are essential for gaining insights into the functional

Address correspondence to Y. Manor, Department of Neurobiology, Institute of Life Sciences, Hebrew University, Jerusalem, 91904, ISRAEL.

role of axonal morphology and physiology. In addition, such studies can help to test hypotheses and suggest critical experiments. Inspired by the pioneering study of Cooley and Dodge (1966), who developed a compartmental modeling approach to simulate the propagation of APs along active cables with Hodgkin and Huxley (H&H, 1952) kinetics, several recent theoretical studies have focused on various aspects of this problem. Hence, local changes in geometry (diameter change and bifurcation), local changes in membrane and cytoplasm properties, local demyelinization, and the effect of a local synaptic input for the processing of APs along axons have been explored. Reviews on these studies can be found in Khodorov and Timin (1975), Waxman (1975), Parnas (1979), and Swadlow et al. (1980). The reader is also referred to recent studies by Stockbridge (1989*a*), Segev (1990), and Lüscher and Shiner (1990*a, b*). Although important insights regarding the effect of such local inhomogeneities on the electrical behavior of axons were gained from these studies, they failed to analyze the behavior of APs along realistically complex axons, mainly because of a lack of an appropriate modeling tool that was specifically designed to handle such cases.

One problem in constructing a tool for modeling large axonal trees is the heavy computational load expected to arise. Efficient algorithms such as those developed by Hines (1984, 1989; see also Mascagni, 1989) for simulating arbitrary active axonal trees are, therefore, an essential part of such a simulator. Another critical feature required is a convenient input/output representation of the morphology of the modeled tree and of its electrical behavior.

With these in mind, we developed the simulator AXONTREE. This simulator has two modes of computation. The detailed mode implements a multicompartmental modeling approach (see review by Segev et al., 1989), whereby each compartment models an electrically short region of the axon whose membrane obeys H&H-like kinetics. The simulated tree is constructed directly on the screen, using the mouse, and the results of the simulation (coded in colors or in black and white) are presented, on-line, on top of the modeled tree. The efficient numerical improvements suggested by Hines (1984) are implemented together with a novel idea of dynamical lumping of the axon into simpler representations during the simulation. For a given accuracy, the combination of these improvements enables one to simulate highly-branched axons in a reasonable time. The efficiency of different methods of computations both for a single AP and a train of APs is demonstrated using a reconstructed axonal terminal from the area 17 in the visual cortex of the cat (represented by 145 compartments). In the companion paper, a whole axonal tree from the somatosensory cortex of the cat (represented by 2366 compartment) is simulated using AXONTREE.

The more abstract mode of simulation in AXONTREE uses an event-driven modeling approach. The idea is to explore (preprocess) the compartmental model in sufficient detail with the aim of extracting rules that will serve as a basis for the event-driven simulation mode. We start from the details and progress carefully, while retaining the essential features of the model, toward a more abstract (and much faster) simulation. This approach is demonstrated for the case of an AP propagating along complex axonal trees. AXONTREE is available, free of charge, on request.

METHODS

AXONTREE is a simulator for modeling the propagation of Hodgkin and Huxley (H&H)-like APs along complicated axonal trees. The program is written in C for the SUN family of workstations under the SUNVIEW as well as the X11 window environments. In general, the simulator consists of three major modules: (*a*) The input module enables the user to interactively construct arbitrary trees on the screen using the mouse, or to load existing files that describe axonal structures. Simultaneously, with the construction of an axon on the screen, a data base representing the axon morphology is built in memory; (*b*) the computing module performs the actual simulation. The simulation can be implemented at two different levels: the detailed level of compartmental modeling, and the more abstract level of event-driven simulation; and (*c*) the output module displays the results in an on-line graphical form by superimposing the voltage distribution on the image of the axon. The results of the analysis can also be stored in tabular form. The details of each of these modules will be elaborated below, after a short description of the user interface capabilities of AXONTREE.

User interface

AXONTREE's screen main window contains a graphical window and a control panel (Fig. 1). The former is used for constructing the modeled axon, selecting sites for "probes" or "electrodes", and for displaying the results. The latter consists of ten mouse-activated icons, some operating as menus and some as simple command buttons. The main features available when these icons are activated are summarized below:

RUN: running the simulation, or resuming it (after a user-activated interrupt).

SCREEN: resetting or changing the screen configuration. Options available include clearing the screen; changing from 8 bit graphics (256 colors) to 1 bit graphics (monochrome) and vice versa; showing or hiding the on-line graphical output, etc.

OUTPUT: chooses those model variables to be saved for further processing. For example, a table of the voltage in the time domain at a given probe, or a table of the voltage in the spatial domain at a given time, etc.

FILES: loading or storing axonal data from, and to, external files.

BYE: quit the program.

CHANGE: changing integration parameters (Δx, Δt, end-time), modifying membrane and axoplasm characteristics (C_m, $\bar{g}$Na, R_i, etc.) either for the whole tree or for each compartment separately, changing the rate equations (αs and βs), adding myelin at different regions of the

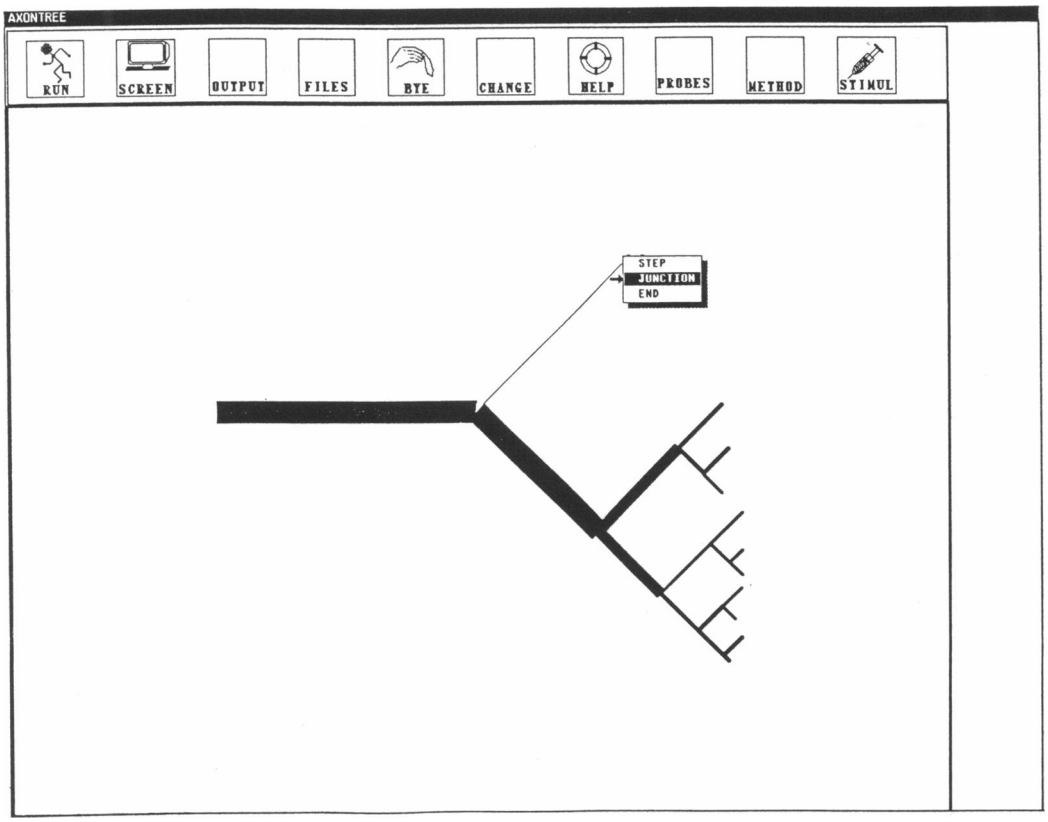

FIGURE 1 Interactive construction of an axonal tree using AXONTREE. The simulator is a graphically based application running within a window. It consists of two major subwindows. The upper subwindow is a control panel consisting of ten buttons (icons), which are used to change parameters or to send commands to the program. A more detailed description of these buttons is given in the text. The lower part is a graphic window in which the axon is constructed and displayed. The tree is built branch after branch. The start point of a branch is the end point of the previously constructed branch. The diameter is set by the value of a global parameter which can be modified at any time by popping up a slider and setting a new value (not shown). A small arrow on the screen, the screen pointer, traces the mouse motions. A branch is constructed by dragging the mouse in a specific direction. A line links the starting point of the branch with the location of the screen pointer. The electrotonic or morphological length represented by the line is displayed (not shown). At any point, the user may choose to terminate the branch; a menu pops up where the termination type is defined either as a bifurcation point (JUNCTION), a diameter change (STEP), or an end (END). Upon selection, a rectangle will be drawn between the initial point and the termination point with a width proportional to the diameter.

axon, etc. This option also permits changing the zoom factors by which the simulated axon is displayed on the screen.
HELP: short description of commands and options.
PROBES: querying the physiological state of the axon at the sites of the probes (e.g., membrane potential, membrane current, ionic conductances, etc.), as well as morphological characteristics (diameter, length).
METHOD: choosing different numerical techniques for enhancing the computation speed. Such methods include the use of predefined tables of rate parameters, dynamic lumping of the axon, second-order accuracy, etc. (see below), as well as choosing the mode (compartmental or event-driven) of simulation.
STIMUL: defining the stimulus parameters (amplitude, duration, frequency of stimulating current).

Input module

Interactively constructing the axon. An example of the method by which the axon is interactively constructed on the screen is depicted in Fig. 1. The axonal tree is composed of cylindrical segments; each segment is constructed on the screen by dragging the mouse on the mouse pad. At any point, the user may choose (by clicking on the left button of the mouse) how the segment terminates: with a step change in diameter; a bifurcation; or a "sealed end". The diameter of the segment has a default value that may be modified by clicking the right mouse button. This opens a window in which the new diameter can be determined.

The tree is constructed in a "depth-first" order. Namely, at any branch point in the tree, one of the daughter branches (and all its descendants) is constructed, and only then is the sibling branch (with all its descendants) built. Simultaneously, with construction of the axon on the screen, an internal data structure (described below) is built in memory.

The data structure. The data structure consists of four interlinked components: a computational tree; a list of terminals; a compressed tree; and a screen-memory map.

The computational tree is the implementation of the compartmental model of the axon. In this model, the axon is subdivided into

electrotonically short isopotential compartments (see Computing module below). For each compartment, a record is dynamically allocated during the construction process. Such a record consists of different fields, storing physiological data (diameter, length, ionic conductances, etc.), graphical data (giving access to the pixels representing the compartments), and addressing information (e.g., links to adjacent compartments). Connections between compartments are made according to the types of the compartments. For example, a prebifurcation compartment is connected to one "father" compartment and two "daughter" compartments. A terminal compartment is connected to one "father" compartment only, etc. This data structure is used to compute numerically and display the voltage distribution along the simulated axon.

The list of terminals consists of pointers to the internal entities (records) representing the terminal compartments in the computational tree. This list is essential, because some of the computations are performed recursively, starting from the terminal compartments toward the initial compartment (see below). Moreover, terminal regions may frequently be accessed by the user: the synaptic (release) site, as well as presynaptic inputs, usually occur at the terminal segments. It is therefore important to keep track of their physiological behavior. Hence, quick access to the terminal records is advantageous both for input/output purposes and for computational efficiency.

The compressed tree is a compact description of the axon. In this description, each uniform section (segment) of the axon (which may be composed of several compartments) is represented by one record. Such records are linked to each other according to the topology of the axon. Links also exist in both directions between a given record in the compressed tree and the corresponding compartments in the computational tree. Hence, information shared by all compartments in the same segment (such as diameter) may be stored only at the level of the compressed tree in order to save memory. This feature is especially convenient when the axon is simplified as a group of delay units and the simulation is performed in an event-driven mode (see Discussion).

The screen-memory map links the graphical display to the compartmental representation. The screen is logically divided into squares of 50×50 pixels. A list of all the segments in the tree that intersect (or are included in) each square is built. A segment may be assigned to several such lists. This procedure links the graphical display of the axon to its computational representation. By pointing to a desired location on the screen one selects a square which is used to access the corresponding list of axonal segments. A specific segment within this list is chosen if the (x,y)-coordinates of the pixel being pointed at are included in it. From there, the appropriate compartment in the computational tree is directly accessed. The user can then modify the compartment parameters or look at its physiological state. This feature also enables the user to edit the tree (add or delete compartments, branches, or subtrees).

Output module

AXONTREE was implemented for the families of SUN workstations where each pixel can be represented either by one bit (monochrome) or by eight bits. In the latter case, each screen pixel can be assigned values between 0 and 255. Each such value codes for a particular color, defined by the programmer as a specific combination of red, green, and blue intensities. Voltage spread along the axon is visualized with this set of colors (see Fig. 4). Membrane potentials are coded in colors, from dark blue (0) for $E_K = -12$ mV to dark red (255) for $E_{Na} = 115$ mV (both relative to the resting potential which was set to zero in this study). Colors are assigned to intermediate voltages by linear interpolation between the range of color codes and the range of voltages. Hence, the midpoint of each compartment is colored according to its membrane potential. In order to create the illusion of a continuous simulation, the interval between two adjacent midpoints is filled with an intermediate range of colors. Color updating is performed only in those compartments where the voltage has changed.

On a monochrome display, a voltage value is defined, above which the appropriate compartments are painted in black. By default, this value is 20 mV depolarization relative to the resting potential. The value can be modified by the user.

Computing module

This module performs the actual computations. When the simulation uses the detailed mode (as opposed to event-driven mode), the compartmental approach is used. Here, the Hodgkin and Huxley (1952; H&H) equations govern the electrical properties of each compartment. The computing module can also perform the computation in event-driven mode which will be discussed only briefly in this study. The compartmental approach in neuronal modeling (Fig. 2) was first suggested by W. Rall (1964) and was recently reviewed by Segev et al. (1989); its implementation for axonal propagation was originally proposed by Cooley and Dodge (1966), used later by many others (e.g., Moore and Ramon, 1974; Parnas et al., 1976; Joyner et al., 1978; Parnas and Segev, 1979; Carnevale and Lebeda, 1987; Stockbridge, 1989a), and recently reviewed by Mascagni (1989).

This section will not repeat the description of this approach. Rather, only the modifications implemented in AXONTREE for the efficient simulation of large and complex trees are treated in more detail. The idea behind these modifications was to develop an algorithm for solving the spread of voltage along the tree such that the computation time will depend only on the number of compartments by which the tree is represented, and not on the complexity of the tree. This is in contrast to algorithms that are commonly used (e.g., Cooley and Dodge, 1966; Parnas and Segev, 1979), where the efficiency decreases as the complexity of the simulated tree increases.

Following the description of compartmental modeling in AXONTREE, a novel method for representing the axon in a simpler form ("dynamic lumping") during the compartmental simulation is pre-

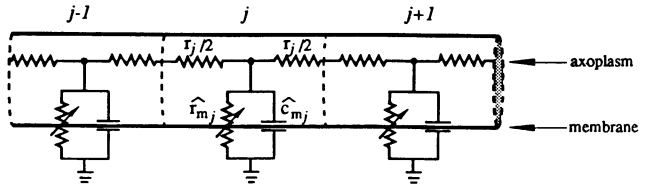

FIGURE 2 Compartmental model of a continuous region of an axon. The equivalent electric circuit is superimposed on the modeled axon. Three successive compartments, labeled $j-1$, j, and $j+1$, are connected in series. Dashed vertical lines show the boundaries between compartments. The membrane of each compartment is modeled as a lumped R-C element connected to other compartments through an axial resistance (the axoplasm resistance). For example, the whole membrane resistance of compartment j is lumped to one variable resistor ($\hat{r}_{mj}$ in Ω), representing the voltage and time dependence of the membrane resistivity (the corresponding ion batteries were omitted in the figure). The membrane capacitance of this compartment is lumped into one capacitor ($\hat{c}_{mj}$ in Farad). The axial resistance in compartment j is modeled by r_j; the membrane elements are placed at the center of this resistance. Hence, the axial resistance between compartments j and $j+1$ is the sum of half the axial resistance in compartment j ($r_j/2$) and half the axial resistance in compartment $j+1$ ($r_{j+1}/2$).

sented. This section ends with a brief discussion of the event-driven level of simulation presently available in AXONTREE.

The detailed level: a compartmental modeling approach. The spread of voltage along axonal trees is described using the one dimensional cable equation (Hodgkin and Huxley, 1952; Rall, 1959, 1977):

$$\frac{a}{2R_i}\frac{\partial^2 V}{\partial x^2} = C_m\frac{\partial V}{\partial t} + I_{ion}(V,t), \tag{1}$$

where V is the voltage difference across the membrane (in mV), a is the axon diameter (in cm), R_i is the specific axial resistivity (in Ωcm), x is the distance along the axon (in cm), t is time (in seconds), C_m is the specific membrane capacitance (in $\mu F/cm^2$) and I_{ion} is the density of the ionic current that flows through the membrane (in $\mu A/cm^2$). In the H&H model this current is given by:

$$I_{ion} = \bar{g}_{Na}m^3h(V - E_{Na}) + \bar{g}_K n^4(V - E_K) + g_L(V - E_L), \tag{2}$$

where g_L is the leak conductance, $\bar{g}_{Na}/\bar{g}_K$ are the maximal ionic conductances of sodium and potassium, respectively (in mS/cm^2), and m, h, n are dimensionless activation and inactivation variables. Each of these variables is governed by the following differential equation:

$$\dot{x} = \alpha_x - (\alpha_x + \beta_x)x; \qquad x = n, m, h, \tag{3}$$

where the dot denotes differentiation with respect to time and α_x and β_x are empirical functions that depend in a rather complicated way on the membrane potential and on the temperature.

The nonlinear partial differential equation (PDE) model of Eq. 1–3 can be solved only by numerical methods. In principle, AXONTREE follows the numerical scheme suggested by Cooley and Dodge (1966), and later implemented for an axon with a single bifurcation by Parnas and Segev (1979). In both cases, a modified Euler predictor-corrector method was used. As will be discussed below, a modification of the Cooley and Dodge (1966) algorithm was essential to handle the highly branched structures that AXONTREE is intended to model.

In compartmental modeling the PDE model of Eqs. 1–3 is made discrete in space ($dx \to \Delta x$), producing a set (or a matrix) of M coupled ordinary differential equations (ODEs), where M is the number of compartments in the modeled axon (see Fig. 2). The matrix of ODEs is solved numerically using finite difference methods. In an unbranched axon, this matrix is strictly tridiagonal, and a simple Gaussian elimination (forward elimination with back substitution) can be employed (Carnevale and Lebeda, 1987). Such an elimination requires $O(M)$ arithmetic operations (i.e., the number of operations is a linear function of M).

In a branched system, however, the discretization of the PDE results in a matrix that is not strictly tridiagonal; it has several nonzero far off-diagonal elements (Hines, 1984; Mascagni, 1989). The number of these far off-diagonal elements depends on the complexity of the tree and may severely reduce the efficiency of the computation. An efficient use of Gaussian elimination that still retains $O(M)$ mathematical operations can be obtained, however (as discussed by Hines, 1984; and Mascagni, 1989), if the elimination procedure progresses in a particular order depending on tree structure. Adopting this idea, we found that for our purposes the most natural order of elimination should start from the terminal tips of the axon (where "sealed end" boundary conditions are assumed) and then progress backwards towards the origin, just in the reverse order in which the tree was constructed (see Input module, above). Using this approach, we then proceed to forward substitute, starting from the origin (where a symmetrical boundary condition around the injection point was assumed; i.e., $V_1 = V_{-1}$), moving along towards the terminals. This procedure results in the following simple algorithm: for any compartment j that is not a pre- or postbifurcation compartment, the membrane potential V_j is

$$V_j = \chi_j + \Gamma_j V_{j-1}, \tag{4}$$

where

$$\chi_j = \frac{\Gamma_j}{D_{j-1}}(B_j + D_{j+1}\chi_{j+1}); \Gamma_j = \frac{D_{j-1}}{A_j - D_{j+1}\Gamma_{j+1}}. \tag{5}$$

For the prebifurcation compartment **L**,

$$V_L = \chi_L + \Gamma_L V_{L-1}, \tag{6}$$

where

$$\chi_L = \frac{\Gamma_L}{D_{L-1}}(B_L + Z^S_{L+1}\chi^S_{L+1} + Z^B_{L+1}\chi^B_{L+1});$$

$$\Gamma_L = \frac{D_{L-1}}{A_L - Z^S_{L+1}\Gamma^S_{L+1} - Z^B_{L+1}\Gamma_{L+1}}, \tag{7}$$

and the superscripts **S** and *B* denote the two daughter branches.

For the postbifurcation compartment in the daughter branch **S**,

$$V^S_{L+1} = \chi^S_{L+1} + \Gamma^S_{L+1}V_L, \tag{8}$$

where

$$\chi^S_{L+1} = \frac{\Phi^S_{L+1}\psi^B_{L+1} + \psi^S_{L+1}}{1 - \Phi^S_{L+1}\Phi^B_{L+1}}; \Gamma^S_{L+1} = \frac{\Phi^S_{L+1}\xi^B_{L+1} + \xi^S_{L+1}}{1 - \Phi^S_{L+1}\Phi^B_{L+1}}$$

$$\Phi^S_{L+1} = \frac{W^{SB}_{L+1}}{A^S_{L+1} - D^S_{L+1}\Gamma^S_{L+2}}; \xi^S_{L+1} = \frac{\Phi^S_{L+1}W^S_{L+1}}{W^{SB}_{L+1}}$$

$$\psi^S_{L+1} = \frac{\Phi^S_{L+1}(B^S_{L+1} + D^S_{L+2}\chi^S_{L+2})}{W^{SB}_{L+1}}$$

$$\Phi^B_{L+1} = \frac{W^{BS}_{L+1}}{A^B_{L+1} - D^B_{L+1}\Gamma^B_{L+2}}; \xi^B_{L+1} = \frac{\Phi^B_{L+1}W^B_{L+1}}{W^{BS}_{L+1}}$$

$$\psi^B_{L+1} = \frac{\Phi^B_{L+1}(B^B_{L+1} + D^B_{L+2}\chi^B_{L+2})}{W^{BS}_{L+1}} \tag{9}$$

and B_j, A_j, D_j, Z^S_{L+1}, Z^B_{L+1}, W^{SB}_{L+1}, W^{BS}_{L+1}, W^S_{L+1}, W^B_{L+1} are defined as in Parnas and Segev (1979). The same holds for the daughter branch *B* (with *B* replacing S in the set of equations in Eq. 9).

It is easy to see that with this algorithm the arithmetic complexity is still only $O(M)$. Namely, the computation time is proportional to the number of the model compartments and independent of the complexity of the tree. As in Parnas and Segev (1979), we used in this study a spatial integration step (Δx) of $\lambda/10$ in all our computations, where λ is the space constant of the segment ($\lambda = \frac{1}{2}(d_j R_m/R_i)^{1/2}$, and d_j is the diameter of the segment). The temporal integration step was chosen to be 10 μs. All calculations were performed using a convergence criterion of 10^{-4} mV in the predictor-corrector scheme.

As will be shown below (Tables 1 and 2), compartmental modeling can be time consuming even when a powerful computer is available. In order to increase the computation speed with compartmental modeling, we also used the following techniques.

(*a*) In the H&H model, the rate constants α,β are exponential functions of membrane potential. Because the computation of an exponent is a costly operation (in terms of computation time), a faster simulation is obtained if the rate constants are precomputed and stored in tables. During the actual simulation, the rate constants are evaluated by looking for nearby values in these tables. Accuracy is enhanced by interpolating table values (Hines, 1984).

(*b*) Evaluation of membrane potential at a half time step ($\Delta t/2$)

TABLE 1 **The efficiency of different computational methods**

Case	Computation method (no graphics)	Computation time
		s
1	Full computation	540
2	α, β tables	205
3	Second order accuracy	220
4	Cases 2 + 3	100
5	Dynamic lumping	280
6	Cases 2 + 3 + 5	51

The calculation was performed for a single action potential, traveling along the tree displayed in Fig. 5 A for a total simulation time of 5 ms (with Δt = 10 μs), at a temperature of 20°C, using the SUN 3-60 machine. Case 1 (*full computation*) denotes the case where the complete (unlumped) compartmental model, using a first order predictor-corrector scheme without any numerical improvements, was employed (145 compartments). Case 2 denotes the case where precalculated tables for the rate functions at an interval of 0.1 mV were used. In case 3, the method of Hines (1984) with second order accuracy was used (see Methods). In case 5, dynamic lumping of the axon (with a unlumping criterion of 5 mV) was employed, as demonstrated in Fig. 4. For each case, the computation time (without any graphical output) is given in the right column in seconds. The table shows that efficiency is increased by a factor of 10 when all methods are combined simultaneously.

apart from the evaluation of membrane current results in a second order accuracy approximation (Hines, 1984). This speeds up the computation, because a smaller number of iterations is required to converge at a stable solution. Moreover, the approximation error is smaller than the error obtained when a simple first order accuracy method is used. Thus, larger time steps can be used without loss of accuracy.

Dynamic lumping

As mentioned above, and demonstrated in Tables 1 and 2, the computation of a large compartmental model is time consuming. We will show, however, that under certain conditions the morphological details of particular regions of the simulated axon are not important for the behavior of the AP, and in many instances these details can be "lumped" into a simpler representation (with a smaller number of compartments). For example, when the AP propagates along the main axonal trunk, its behavior is essentially insensitive to the detailed structure of electrically distant terminals. During this time, a simpler representation of the terminals that approximately preserves their conductance and capacitative load can be used to save computation time. This idea was inspired by the work of W. Rall (1959) who showed that, under the following constraints, a whole dendritic tree is electrically equivalent to a single cylinder.

- The specific membrane and axial resistivities are uniform along the tree. In the case of an excitable membrane, both the voltage-dependent as well as the passive membrane characteristics (per unit area) should be uniform along the tree (Goldstein and Rall, 1974; Parnas and Segev, 1979).
- At any branch point,

$$\sum_i d_i^{3/2} = d_p^{3/2},$$

where d_i are the diameters of the daughter branches, and d_p is the diameter of the parent branch. In other words, the geometrical ratio (GR) is equal to unity

$$GR = \frac{\Sigma_i d_i^{3/2}}{d_p^{3/2}} = 1. \quad (10)$$

- The electrotonic distance ($X = x/\lambda$) from the soma to all dendritic terminals is the same.
- The boundary conditions are identical at all dendritic terminals.

Satisfying these conditions, the voltage time course in the dendritic (or axonal) tree can be mapped onto an equivalent cylinder by means of the electrotonic distance, X, measured from the origin, $X = 0$ (Rall, 1959, 1989).

In cases where the equivalent cylinder criteria are not satisfied, a tree (or a subtree) can still be approximated by a simplified model: the "equivalent profile" or the "equivalent cable" (see Fleshman et al., 1988; Clements and Redman, 1989; Stratford et al., 1988). Unlike a cylinder, the diameter of such a profile may vary along its length. The profile is constructed using the following procedure.

First, all branches are normalized in units of X. Then, the diameters ($d_i(X)$) at all points lying at an identical electrotonic distance (X) are lumped to an "equivalent" diameter ($d_{eq}(X)$) using the equation:

$$d_{eq}(X) = \left\{\sum_i d_i(X)^{3/2}\right\}^{2/3}. \quad (11)$$

An example of lumping a simple tree consisting of a single bifurcation into an "equivalent" cable is schematically shown in Fig. 3. In this simple example the original tree is composed of a parent branch (p) and two daughter branches (b_1, b_2), unequal in both their diameters and cable lengths. The "equivalent" cable to this tree consists of three cylinders, the first (c_1) is identical to the original branch p. The middle cylinder is composed of the two daughter branches in the original tree.

TABLE 2 **Computation times for different frequencies of stimulation**

Stimulation frequency	Full computation	Dynamic lumping	Gain
Hz	*s*	*s*	%
0	727	232	68
20	760	258	66
50	825	308	63
100	888	358	60
200	986	460	53
300	1030	507	51

The axon displayed in Fig. 5 A was simulated at various frequencies (column 1) for 50 ms (5,000 time steps), using the full compartmental method (column 2) or the dynamic lumping technique (column 3). Column 4 shows the gain in computation time achieved using the dynamic lumping technique, compared with the full compartmental method. At 0 frequency no spike was initiated and the axon was represented in the dynamic lumping method by a single "equivalent" cylinder (45 compartments) during the whole simulation time. In the full computation method the original tree (145 compartments) was employed during the whole simulation. The 68% gain in computation time in the 0 frequency corresponds closely to the ratio of compartments used for the simulation in the two respective cases (i.e., 1 − [45/145]). As the stimulation frequency increases, the axon is represented by progressively more complicated "equivalent" cables and the gain in computation time that results from dynamical lumping of the axon decreases. Nevertheless, even at high frequency of 300 Hz, the gain in computation time is 51%.

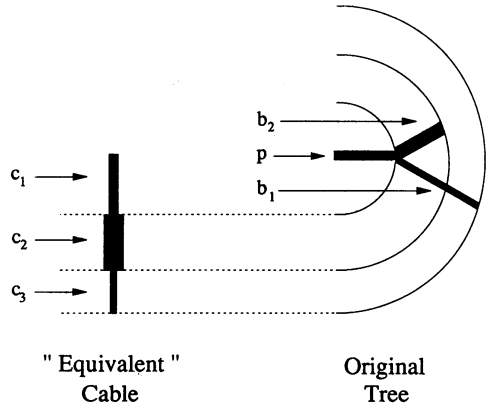

FIGURE 3 Construction of an "equivalent" cable approximation for an arbitrary axonal (or dendritic) tree. In this example, the original tree (given in units of λ) consists of a parent branch (p) and two daughter branches (b_1 and b_2) with different electrotonic lengths ($b_1 > b_2$). The "equivalent" cable is composed of three successive cylinders, c_1 to c_3. The diameter of c_1 is equal to the diameter of the parent branch p. The diameter of c_2 is equal to $(b_1^{3/2} + b_2^{3/2})^{2/3}$, whereas the diameter of c_3 is equal to the diameter of b_1. Curved and dashed lines denote points with identical electrotonic distances, X (see text for more details).

Its diameter is calculated from Eq. 11 and its cable length is identical to that of branch b_2. The third cylinder (c_3) has the same diameter as b_1; its cable length is the difference between the cable lengths of b_1 and b_2.

Fleshman et al. (1988), Clements and Redman (1989), and Stratford et al. (1989) have shown that for transients measured at the soma, this approximation of the dendritic tree is satisfactory. Hence, from the soma viewpoint, the "equivalent" cable is a reasonable simplification which markedly speeds up the computation (because the axonal or dendritic tree is modeled by a significantly smaller number of compartments). They noted, however, that from other points of view (e.g., when the input as well as the point of observation are both at a distal dendritic site) this approximation is inappropriate. In such cases the morphological details near the region of interest should be represented in full.

These insights, and the fact that the locations of AP firing are continuously changing, have led us to develop a computational method to construct simplified representations that are altered dynamically depending on the location of the spike along the tree. Hence, axonal regions that are currently active (that fire an AP) are fully represented, whereas other regions are represented by "equivalent" cables. An example of the implementation of this method is given in Fig. 4. When the AP propagates along the main axonal trunk, distal parts of the tree are lumped to a single cable according to Eq. 11 (see Fig. 4 *A*). Let X be a point where a bifurcation exists in the original tree. As the voltage at X reaches a critical depolarization, the cable is "unlumped" into a more detailed structure consisting of a parent branch and two daughter branches (Fig. 4 *B*). In this case, with an unlumping criterion (V_{unlump}) of 5 mV depolarization, the "unlumping" takes place when the AP peak is at 0.8 λ proximal to the branch point. The daughter branches are not represented with their original diameters, although their descendants are still modeled by their respective "equivalent" cables. More distal regions of the tree are restored, in turn, when invaded by the AP (Fig. 4, *C* and *D*).

This process of unlumping the axon back into its full representation is accompanied by relumping terminal branches belonging to the same subtree into their "equivalent" cable, provided that the AP there (in all terminals) has already peaked (Fig. 4, *E* and *F*). This "equivalent" cable is assigned a voltage profile identical to that of the electrically longest branch. The relumping starts at the terminal branches and gradually processes backward until a single cable representation is again reached (Fig. 4 *F*). A complete relumping of the tree into a single cable, however, may not take place if another AP is initiated before this stage is attained. Note that, when a train of APs is simulated, the relumping process may introduce an error in two cases.

(*a*) An AP may invade a relumped bifurcation (a bifurcation point whose daughter branches have been relumped into one "equivalent" cable) which is still depolarized (from previous spikes) beyond the value of V_{unlump}. In this case the whole postbifurcation tree remains lumped and is erroneously (when the AP propagates through it) treated as a single cable.

(*b*) There is a time window during which, as a result of a previous spike, the voltage at a relumped bifurcation point is below V_{unlump}, yet the voltage along the postbifurcation tree is larger than V_{unlump}. If during this time window an AP approaches the relumped bifurcation point, it will cause the "equivalent" cable to unlump. In this case, the assignment of the voltage profile of the "equivalent" cable to the daughter branches may lead to a consistent error. Nevertheless, these two cases are relevant only for very high spike frequencies. Thus, for most realistic cases, they are unlikely to happen.

In AXONTREE, the "equivalent" cable is unlumped at branch points according to a user-defined depolarization value at the branch point (V_{unlump}). For example, if V_{unlump} is set to 20 mV, then only when the bifurcation point at X (in the original tree) is depolarized by more than 20 mV does the unlumping actually occur at that point. A small V_{unlump} value will bring about unlumping sooner than necessary. On the other hand, a large V_{unlump} value will cause severe errors. For example, when one daughter branch is electrically much shorter than the other, the voltage profile along these branches is not identical. Unless V_{unlump} is sufficiently small, the unlumping procedure (in which the two daughter branches are assigned the voltage profile of the "equivalent" cable) will introduce an error. Our experience from simulating many axonal trees indicates that a V_{unlump} of 5 mV is optimal; the computation becomes more efficient (see Tables 1 and 2) with only a minor cost in accuracy (less than 1%).

In a typical simulation (unlike the case of Fig. 4), when the method of dynamic lumping is chosen (with the METHOD menu, see above), the process of dynamic lumping is hidden from the user. The structure displayed on the screen is the original tree. At each time step, voltage distribution is computed on the simplified representation (stored in memory) and then mapped onto the original structure.

An interesting point to note in relation to Fig. 4 is concerned with the spatial spread of the AP. The figure shows that the AP fires simultaneously a large region of the axon. For example, in the lower branch of Fig. 4 *C*, the active red region (more than 55 mV depolarization) occupies more than 1 λ of that branch. Hence, the AP is a relatively broad wave of excitation, as it spreads along the axon.

Event-driven simulation. As noted above, AXONTREE, in addition to the detailed compartmental level, also allows a more abstract mode of simulation, the event-driven mode. This mode will not be elaborated in this study. Because we believe that for large and complex axons, especially when neural networks with many such axons are modeled, event-driven simulations will eventually replace the detailed mode of compartmental modeling, it is worthwhile to describe this approach briefly here.

The idea is to explore in depth the detailed mode, which solves the cable PDE, in order to formulate rules upon which the more abstract, event-driven, mode of computation is based. Presently, AXONTREE implements such a mode for computing the propagation delay of a

single AP along arbitrary axonal trees. Using the compartmental model (see companion paper), we found that for most practical purposes the axonal tree can be decomposed into four types of "delay boxes."

(*a*) A uniform region of the axon.

(*b*) A site with $GR \neq 1$ (a step change in diameter or a branch point).

(*c*) Two successive electrically close sites, both with $GR \neq 1$.

(*d*) A terminal.

Study of the results of using the compartmental modeling of AXONTREE allowed us to obtain general rules for: (*a*) decomposing (or "chopping") the tree into a series of "delay boxes" so that the total delay along a path from the origin to the terminal tip will be a linear sum of all the delays in the individual boxes along this path; (*b*) calculating the delay expected in each box. In a uniform segment the delay can be simply calculated because the propagation velocity in such a region is constant. In a box with $GR \neq 1$, a function describing the delay versus *GR* value was computed using the detailed model (see Fig. 3 in the companion paper). A more complicated function was calculated for the third type of box. It describes the delay as a function of the electrotonic distance between two successive *GR* values (note that when the geometrical changes are electrically close, the delays expected in each *GR* separately do not sum linearly; see Fig. 5 in the companion paper).

Using these rules, AXONTREE can almost directly calculate the delays along arbitrary axons (provided that the parameters of the simulated axon are the same as in the axonal structure which were preprocessed for constructing the appropriate rules). Indeed, we have found that for most cases (including the reconstructed axon used in this study; see Fig. 5, and in the companion paper see Fig. 9), only small discrepancies in propagation delays were found when performing the simulation in event-driven mode, compared with the computation with the full compartmental model (less than 5% on average). At present, however, only a single spike (or a train of spikes at low frequency) can be simulated with the event-driven mode in AXONTREE. For handling high frequencies, where the effects of time (refractoriness, ion accumulation, etc.) should be taken into account, a time-dependent variable has to be introduced into each of the delay boxes mentioned above. The construction of such a "state-machine" representation of the axon will be elaborated elsewhere.

RESULTS

The computations performed in this study were all carried out using a terminal part of a reconstructed axon from region 17 in the visual cortex of the cat (Humphrey et al., 1985). The data is from an unmyelinated axonal terminal arborization of a Y cell. It has an initial diameter of 2 μm and consists of 12 terminals; the longest path is ~1 mm. A drawing of this tree in units of λ is depicted in Fig. 5 *A*. Because the electrical proper-

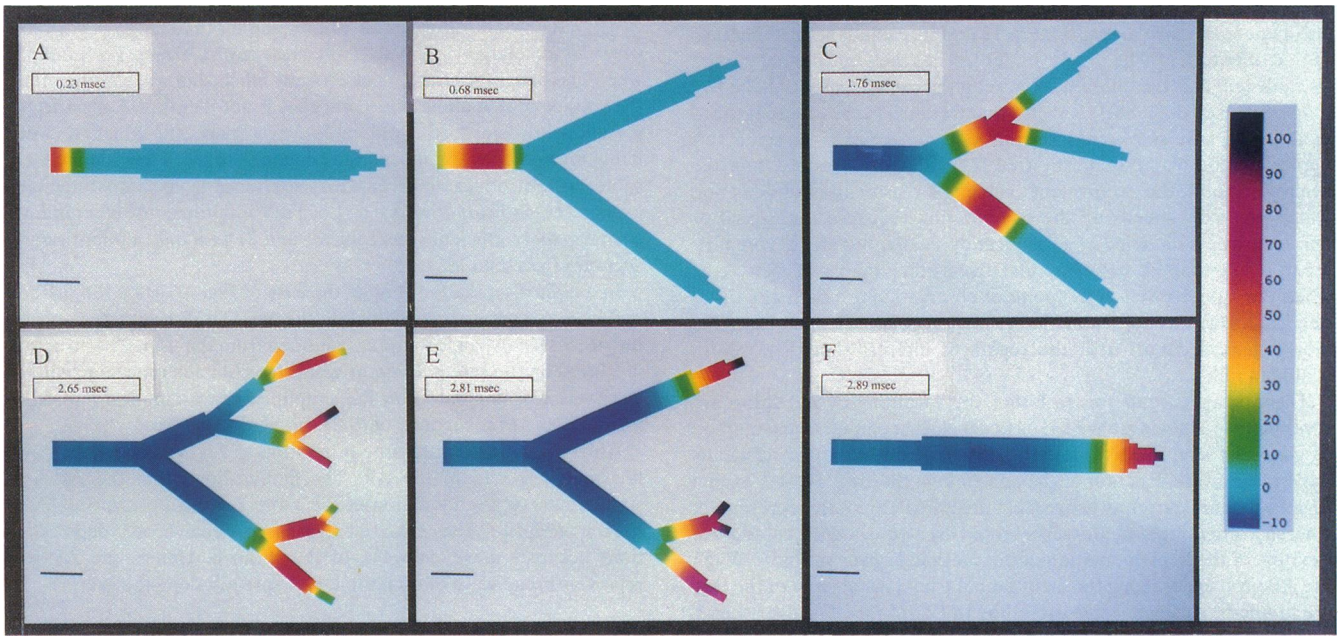

FIGURE 4 Dynamic lumping technique. The modeled axon is represented in simplified forms that are dynamically altered. Each of the six frames (A–F) displays a snapshot of the process. The color scale at the right codes for membrane potential relative to rest. Dark blue represents a hyperpolarization of −12 mV, light blue represents the resting potential (0 mV), and dark red represents a depolarization of 115 mV. The axon time is shown at the top left of each frame. The bar at the lower left corner of each frame calibrates for one space constant (λ). The simulation starts with a single "equivalent" cable representation (*A*). As action potential leading foot (>5 mV) enters the point (*X*), where the original branch exists, the tree is unlumped into one parent branch and two daughter branches; each daughter is represented by the corresponding "equivalent" cable (*B*). The three is progressingly unlumped as the action potential propagates more distally (*C*) until its original structure is fully restored (*D*). As the action potential peaks at the terminals, the corresponding terminals are progressively relumped back into their "equivalent" cable representation (*E*) until the single cable representation is resumed (*F*).

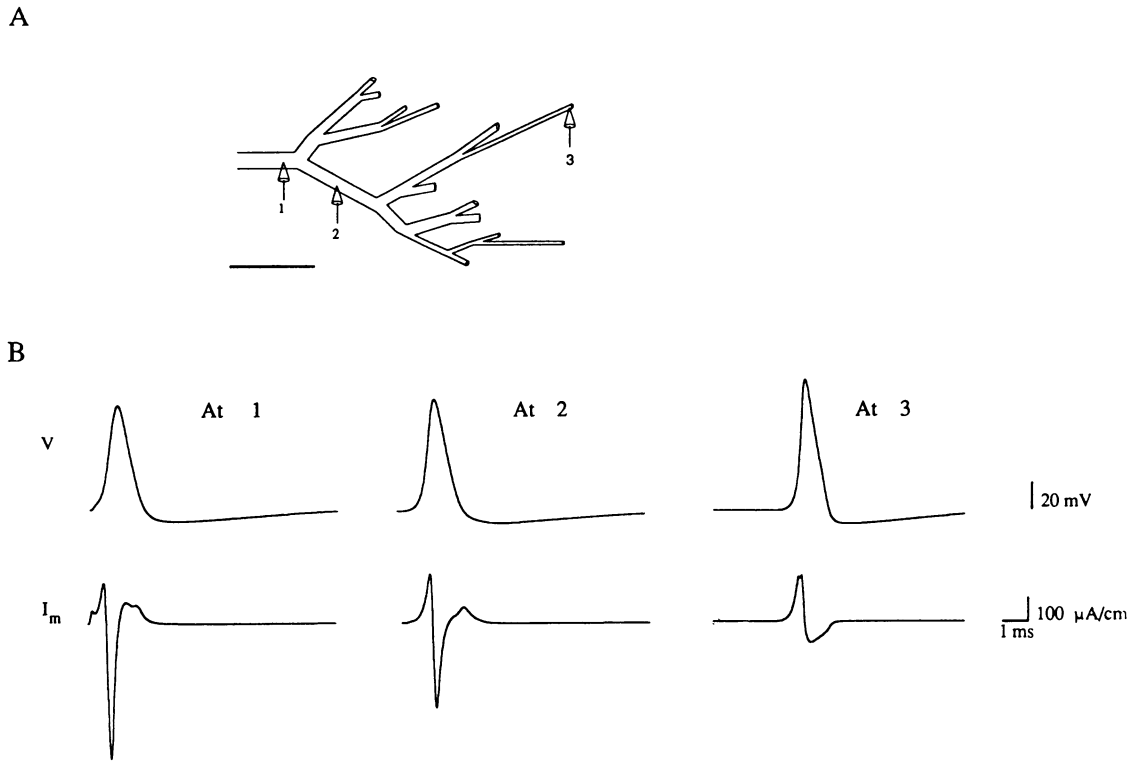

FIGURE 5 The variation in the shape of the action potential and action current along a single axonal tree. In *A*, a terminal portion of a reconstructed axon is displayed in electrotonic units (in units of λ). The bar at the bottom of *A* represents 1λ. "Electrodes" 1, 2, and 3 show the three sites of recording: at the first branching point, at a midpoint along the lower first order daughter branch and at a distal terminal, respectively. In *B*, the membrane potential (V) and the associated membrane current (I_m) are shown at the corresponding sites. As expected near a branch point with $GR > 1$, the action potential is relatively small at point 1 (where $GR = 1.84$) and the associated membrane current appears with an increased inward (negative) phase. The action and current resume their normal shape (as in an homogeneous axon) at point 2. At the terminal (point 3) the action potential velocity and amplitude are relatively large and the current changes from triphasic into biphasic with a predominant outward (positive) phase.

ties of the membrane of these axons are not known, and because we here wish to examine qualitatively the performance of AXONTREE, we have used the kinetics of Hodgkin and Huxley (1952). Namely, The maximal Na^+ and K^+ conductances ($\bar{g}_{Na}$, $\bar{g}_K$) are 120 mS/cm^2 and 36 mS/cm^2, respectively, the leakage conductance (g_L) is 0.3 mS/cm^2, and the specific capacitance, C_m, is 1 μF/cm^2. The simulations were performed at 20°C. These parameters imply a resting membrane resistivity, R_m, of 1,400 Ωcm^2. Together with R_i of 70 Ωcm and a given diameter, the space constant of each segment composing the three can be calculated. As can be seen in Fig. 5 *A*, the longest path is ~4.5 λ. The sum of cable lengths of all branches that compose this tree is 14.5 λ. Hence, because the cable length of each compartment was chosen to be 0.1λ (see Methods), the total number of H&H compartments used to model the whole tree was 145.

In Fig. 5 *B*, the AP (V) and associated membrane current (I_m) at three points along the simulated axon are shown. As seen in Fig. 5 *A*, point 1 is just proximal to the first branch point, where $GR = 1.84$ (a relative increase in diameter). Point 2 is at a point along the lower first order daughter branch, whereas point 3 is at the most distal terminal as shown in Fig. 5 *A*. As expected, the amplitude of the AP near a point with $GR > 1$ (a reduction in safety factor for propagation) is reduced (to 80 mV versus 86 mV in the uniform case). The corresponding membrane current appears with an increased inward current; the reason for this somewhat unintuitive behavior of I_m is discussed by Khodorov and Timin (1975) and Parnas and Segev (1979). Point 2 is along a homogeneous region of the tree and both the AP amplitude as well as the membrane current there are the same as in a uniform axon. At the terminal (point 3), the sealed-end boundary conditions result in an increase in both rise time (slope) and voltage amplitude (see also Goldstein and Rall, 1974). The membrane current at

this point changes from triphasic to biphasic, with an increased outward current (increased capacitative current) and a reduced inward current (decrease in the inward Na current due to the reduction in its driving force), as found experimentally near terminal ends (Katz and Miledi, 1965).

These results show that both V and I_m behave as found using other compartmental models; this convinced us that AXONTREE works appropriately. The next step was to examine different methods to enhance its computational speed.

Table 1 compares the computation time needed to compute 5 ms of axonal time (500 time steps, each 10 μs) using different methods. A single AP was initiated at $X = 0$ (left-most point in Fig. 5 *A*) by injecting a 700 μA depolarizing current for 0.04 ms into the first compartment. Case 1 in Table 1 shows that the computation time was 540 s when the full compartmental model (without any numerical improvements) was employed using the SUN 3-60. Adding color graphics to the computation increased the computation time to 805 s (not shown). When precalculated tables for the rate constants (α,β) at voltage intervals of 0.1 mV were used, the computation time was reduced to only 205 s (case 2). This is a significant improvement (62%) as compared with the full computation (without graphics). We could not detect any noticeable difference between the results using these tables and the full computation. We also tried to use tables with a 1 mV interval; the differences in both computation time and accuracy as compared with an interval of 0.1 mV are negligible. A second order accuracy method (Hines, 1984; and see Methods) helped reducing the calculation time by 59% as compared with the full computation (case 3). Cases 2 and 3 when used together resulted in a reduction of computation time by 81% (case 4). Dynamic lumping (and relumping) of the axon was also proven to be useful in saving computational time (a reduction of 48% relative to the full computation, case 5). Note that the saving in computation time with the lumping method depends on the percentage of time that the axon is "busy" with the AP. Hence, if the axon is electrically short and is activated at low frequency, the axon is fully lumped for a relatively large percentage of the computation time. Otherwise, the axon will be represented in full most of the time. This point is further elaborated on in connection with Table 2.

An impressive improvement in computation time was obtained when all the above methods (2, 3, and 5) were employed simultaneously. For the case examined, only 51 s were needed to complete the computation compared with 540 s in the full computation of case 1 (a factor of ~10). Again, no noticeable differences in both V, I_m, and delay time of the AP in the axon terminals could be detected.

To further explore the contribution of the dynamic lumping technique to the overall increase in computation efficiency, we stimulated the axon in Fig. 5 at several frequencies (Table 2) for a total duration of 50 ms (5,000 time steps). Because the axon consists of 145 compartments in the full compartmental model, and of 45 segments in the single cable representation, the maximal gain in computation time using this method is expected to be $[1 - (45/145)] = 69\%$. Indeed, when no AP was initiated (the tree is at resting potential during the whole computation) and the tree was represented in full (unlumped), the computation time, using the methods 2 and 3 in Table 1, is 727 s. When the dynamical lumping method was employed for this case the computation time was reduced to 232 s (68%) as expected. When only a single AP travels along the axon the computation time is 760 s, compared with 258 s (66%) with dynamic lumping. It should be noted here that the 760 s computation time should be compared to 100 s computation time that was calculated in the corresponding case (of 5 ms) in Table 1 (case 4). If the computation time was linearly scaled with the simulation time, then 1,000 s computation time (rather than 760 s) should have been required to compute 50 ms. The reduction is explained by the fact that when only one spike is computed during a total duration of 50 ms, the axon is quiescent (no steep changes) for a large percentage of time and, on the average, the numerical solution is converged requiring a smaller number of iterations in the predictor-corrector procedure (see Methods).

Increasing the stimulation frequency decreases the relative gain in computation time obtained by dynamically lumping the axon. Even at the high frequency of 300 Hz, however, the gain in computation time is 51%. Hence, even at this rate, parts of the axon are represented more simply during the simulation. On the average, the axon is represented in this frequency of stimulation by ~50% of the original number of compartments, namely by 70 compartments (rather than 145 compartments). In conclusion, the dynamic lumping procedure is a very efficient procedure for enhancing the simulation of APs that travel along complicated axonal trees.

DISCUSSION

In choosing a modeling tool for exploring a particular biological problem there is always the question whether to use a general-purpose simulator or to write a computer program designed to solve the specific set of model equations. The first approach frees the user from writing

the program and allows accommodation of new data and construction of new models in a relatively straightforward manner. This is the case with simulators such as SPICE, SABER, ASTAP, and GENESIS that have been proven useful for neuronal modeling (Shepherd and Brayton, 1979; Segev et al., 1989; Wilson and Bower, 1989; Carnevale et al., 1990; and see also Traub and Wong, 1983). The second approach, whereby the user tailors a program to his specific needs, enables one to make use of the properties of the modeled system and, thus, to save significant computational time and provide convenient input/output capabilities that are essential when one aims at understanding the behavior of large systems. This approach was adapted by De Schutter, 1989 (NODUS), Hines, 1989 (CABLE), and in this paper by us.

The construction of AXONTREE is, indeed, heavily based on known properties of the electrical activity of axons and on the specific structure of the H&H model. Hence, precalculated tables of the voltage-dependent rate functions (Eq. 3) were used as well as the dynamic lumping method. Both were proven to significantly increase computation efficiency. These approaches, together with an algorithm that takes into account the tridiagonal-like structure of matrices that arises from compartmental representation of axonal trees, produced a very fast simulator that can handle large trees. Just to give a gross comparison with other simulators, the simulation of the propagation of a single spike for 20 ms in a chain of 100 H&H compartments using SPICE (which is very efficient for passive models) took ~2 h computation time in the VAX/VMS 750 computer. In SABER, running on the SUN 3-260 (a 4 mips machine) such a model takes ~18 min to simulate (Carnevale et al., 1990). In AXONTREE, the same simulation, using the combined methods of Table 1, takes ~2.5 min on the SUN 3-60 (a 3 mips machine). It is also important to note in this context that we took particular care that the computation time in AXONTREE will be independent of the complexity of the tree. Our experience with SPICE shows that, for a fixed number of compartments and simulated time, the computation time increases as the branching pattern of the simulated system becomes more complicated. We do not have information about SABER or GENESIS performance regarding this point.

Another critical feature of neuronal simulators is the handling of the input data, and the presentation of the simulation's results. We found that it was convenient to construct new trees by using the mouse for defining the desired morphology and the length and diameter of its different segments as well as the membrane properties (channel density, channel kinetics etc.). A good general picture of the behavior of the axon is obtained when the voltage, coded in color, is continuously superimposed on top of the simulated structure (Fig. 4). For obtaining more details, such as the shape of the voltage and the membrane current, the conductance change and the value of the different rate functions; "probes" can be impaled at interesting sites to extract and save the relevant information (Fig. 5).

When building a simulator, special care has to be given to test its results against the results of other, independent, simulators. AXONTREE, in its full compartmental mode, was first compared with the original results to Hodgkin and Huxley (1952). An excellent fit of the value of the threshold (which is very sensitive to numerical errors) as well as of the shape and velocity of the AP was found. Next, the behavior of the AP near regions with low safety factor for propagation (such as near a significant increase in diameter and branch point with $GR \gg 1$) was compared with the results obtained by Parnas and Segev (1979), again with excellent agreement. Trusting the performance of the full compartmental model, its results could then serve as a basis for analysing the different methods that were developed to enhance computation speed. Use of Hines' (1984) numerical method to produce second order accuracy ($O(\Delta t^2)$), the precalculated tables for the rate functions (with a step size of 0.1 mV) and the dynamic lumping method with an unlumping criterion (V_{unlump}) of 5 mV, used together, resulted in a 10-fold decrease in computation time with less than 1% change in the AP parameters mentioned above. We have also tried to progressively cut off the simulated axon, whereby those proximal parts (those compartments) that already reached the AP peak were "removed" from the compartmental representation of the tree. This saves significant computation time when a single AP is simulated; this feature, however, was removed from AXONTREE because it is not useful when modeling trains of APs.

What can one learn from using AXONTREE? Several questions that were not explored previously are now simple to examine. What type of interactions are expected between successive, electrically adjacent, branch points, each having a $GR \neq 1$? For example, how is the delay obtained when the proximal branch point has a particular $GR > 1$ and the more distal one has a $GR < 1$ compared with the delay obtained in the reverse order of GR values? What happens to a high frequency of APs when they approach a region of multiple successive varicosities (release sites)? Does the AP in an actual axon arrive at significantly different times at all its terminals? Clearly, answers to these questions may have important implications for the function of neuronal systems (see Carr and Konishi, 1988) as well as for neuronal models concerned with highly connected neu-

ronal networks (Hopfield, 1982). Some of these issues are tackled in the companion paper (Manor et al., 1991).

Finally, it is clear that the compartmental modeling approach is limited when one wishes to model large neuronal systems for long periods of time in detail. In this case some simplifications are necessary. One such simplification is to reduce the number of compartments representing each neuron to only few compartments (e.g., Traub and Wong, 1983; Wilson and Bower, 1989). Another approach, which is expected to become popular in the near future, is to use parallel machines, each handling only part of the simulated system (e.g., a single compartment, a dendrite, an axonal branch). As noted by Nelson et al. (1989), compartmental models of neuronal structures lend themselves to parallel simulations. The use of relatively cheap array processors was also shown to significantly improve the computation involved in compartmental modeling (Stockbridge, 1989*b*). A third approach, suggested in this study, is to move to a higher and much faster mode of modeling, the event-driven or "state-machine," scheme. In order to retain the essential features of the modeled system, the construction of this level of representation should be based heavily on the functional rules that were formulated as a result of detailed exploration of the compartmental models. Whatever the approach will be, it seems safe to conclude that advances in anatomical and biophysical methods, combined with powerful computers and sophisticated programs, will enable us to construct realistic models, thereby increasing our understanding of the information processing performed by neuronal systems, from the subcellular level of axons, dendrites, spines, to the level of the network.

We are grateful to Professor R. Werman for his helpful comments on an early version of the manuscript.

This work was supported by grants from the National Institutes of Health and Office of Naval Research to Dr. Segev.

Received for publication 16 February 1990 and in revised form 29 April 1991.

REFERENCES

Barron, D. H., and B. H. C. Matthews. 1935. Intermittent conduction in the spinal chord. *J. Physiol. (Lond.)*. 85:73–103.

Bittner, G. D. 1968. Differentiation of nerve terminals in the crayfish opener muscle and its functional significance. *J. Gen. Physiol.* 51:731–758.

Braitenberg, V. 1967. Is the cerebellar cortex a biological clock in the millisecond range? *In* Progress In Brain Research. The Cerebellum. Elsevier, Amsterdam. 334–346.

Carnevale, N. T., and F. J. Lebeda. 1987. Numerical analysis of electrotonus in multicompartmental neuron models. *J. Neurosci. Methods.* 19:69–87.

Carnevale, N. T., T. B. Woolf, and G. M. Shepherd. 1990. Neuron simulations with SABER. *J. Neurosci. Methods.* 33:135–148.

Carr, C. E., and M. Konishi. 1988. Axonal delay lines for time measurement in the owl's brainstem. *Proc. Natl. Acad. Sci. USA.* 85:8311–8315.

Chung, S., S. A. Raymond, and J. Y. Lettvin. 1970. Multiple meaning in single visual units. *Brain Behav. Evol.* 3:72–101.

Clements, J. D., and S. J. Redman. 1989. Cable properties of cat spinal motoneurones measured by combining voltage clamp, current clamp and intracellular staining. *J. Physiol. (Lond.)*. 409:63–87.

Cooley, J. W., and F. A. Dodge. 1966. Digital computer solutions for excitation and propagation of the nerve impulse. *Biophys. J.* 6:583–599.

De Schutter, E. 1989. Computer software for development and simulation of compartmental models of neurons. *Comp. Biol. Med.* 19:71–81.

Fleshman, J. W., I. Segev, and R. E. Burke. 1988. Electrotonic architecture of type identified α-motoneurons in the cat spinal cord. *J. Neurophysiol.* 60:60–85.

Freeman, J. A. 1969. The cerebellum as a timing device: an experimental study in the frog. *In* Neurobiology of Cerebellar Evolution and Development. R. Llinas, editor. Chicago. 397–420.

Fyffe, R. E. W., and A. R. Light. 1984. The ultrastructure of group Ia afferent fiber synapses in the lumbosacral spinal cord of the cat. *Brain Res.* 300:201–209.

Goldstein, S. S., and W. Rall. 1974. Changes in action potential shape and velocity for changing core conductor geometry. *Biophys. J.* 14:731–757.

Grossman, Y., I. Parnas, and M. E. Spira. 1979. Differential conduction block in branches of a bifurcating axon. *J. Physiol. (Lond.)*. 205:283–305.

Hille, B. 1984. Ionic Channels of Excitable Membranes. Sinauer Associates, Inc. Sunderland, MA. 446 pp.

Hines, M. 1984. Efficient computation of branched nerve equations. *Int. J. Biomed. Comput.* 15:69–76.

Hines, M. 1989. A program for simulation of nerve equations with branching geometries. *Int. J. Biomed. Comput.* 24:55–68.

Hodgkin, A. L., and A. F. Huxley. 1952. A quantitative description of membrane current and its application to conduction and excitation in nerve. *J. Physiol. (Lond.)*. 215:283–320.

Hopfield, J. J. 1982. Neural networks and physical systems with emergent collective computational properties. *Proc. Natl. Acad. Sci. USA.* 79:2554–2558.

Humphrey, A. L., M. Sur, D. J. Uhlrich, and S. M. Sherman. 1985. Projection patterns of individual X- and Y-cell axons from the lateral geniculate nucleus to cortical area 17 in the cat. *J. Comp. Neurol.* 233:159–189.

Jahromi, S. S., and H. L. Atwood. 1974. Three dimensional ultrastructure of the crayfish neuromuscular apparatus. *J. Cell. Biol.* 63:599–613.

Joyner, R. W., M. Westerfield, J. W. Moore, and N. Stockbridge. 1978. A numerical method to model excitable cells. *Biophys. J.* 22:155–170.

Katz, B., and R. Miledi. 1965. Propagation of electric activity in motor nerve terminals. *Proc. R. Soc. Lond. B.* 161:453–482.

Khodorov, B. I., and E. N. Timin. 1975. Nerve impulse propagation along nonuniform fibres (investigations using mathematical models). *Prog. Biophys. Molec. Biol.* 30:145–184.

Kisvarday, Z. F., K. A. C. Martin, M. J. Friedlander, and P. Somogyi. 1987. Evidence for interlaminar inhibitory circuits in the striate cortex of the rat. *J. Comp. Neurol.* 260:1–19.

Lüscher, H.-R., and J. S. Shiner. 1990*a*. Computation of action potential propagation and presynaptic bouton activation in terminal arborizations of different geometries. *Biophys. J.* 58:1377–1388.

Lüscher, H.-R., and J. S. Shiner. 1990*b*. Simulation of action potential propagation in complex terminal arborizations. *Biophys. J.* 58:1389–1399.

Manor, Y., C. Koch, and I. Segev. 1991. The effect of geometrical irregularities on propagation delay in axonal trees. *Biophys. J.* 60:1424–1437.

Mascagni, M. V. 1989. Numerical methods for neuronal modeling. *In* Methods in Neuronal Modeling. From Synapses to Networks. C. Koch and I. Segev, editors. MIT Press. 439–481.

Moore, J. W., and F. Ramon. 1974. On numerical integration of the Hodgkin and Huxley equations for a membrane action potential. *J. Theor. Biol.* 45:249–273.

Nelson, M. E., W. Furmanski, and J. M. Bower. 1989. Simulating neurons and networks on parallel computers. *In* Methods in Neuronal Modeling. From Synapses to Networks. C. Koch and I. Segev, editors. MIT Press. 397–437.

Parnas, I. 1972. Differential block at high frequency of branches of a single axon innervating two muscles. *J. Neurophysiol.* 35:903–914.

Parnas, I. 1979. Propagation in nonuniform neurites: form and function in axons. *In* The Neurosciences, Fourth Study Section. F. O. Schmidtt and F. G. Worden, editors. MIT Press. 499–511.

Parnas, I., S. Hochstein, and H. Parnas. 1976. Theoretical analysis of parameters leading to frequency modulation along an inhomogeneous axon. *J. Neurophysiol.* 89:909–923.

Parnas, I., and I. Segev. 1979. A mathematical model for conduction of action potentials along bifurcating axons. *J. Physiol. (Lond.)*. 295:323–343.

Rall, W. 1959. Branching dendritic trees and motoneurone membrane resistivity. *Expt. Neurol.* 2:503–532.

Rall, W. 1964. Theoretical significance of dendritic tree for input-output relation. *In* Neural Theory and Modeling. R. F. Reiss, editor. Stanford University Press. 73–97.

Rall, W. 1977. Core conductor theory and cable properties of neurons. *In* Handbook of Physiology. The Nervous System. E. Kandel, editor. Bethesda, MD. 39–97.

Rall, W. 1989. Cable theory for dendritic neurons. *In* Methods in Neuronal Modeling. From Synapses to Networks. C. Koch and I. Segev, editors. MIT Press. 9–62.

Raymond, S. A., and J. Y. Lettvin. 1969. Influences on axonal conduction. *In* Quart. Progress Report No. 92, Research Laboratory of Electronics. MIT. 431–435.

Rockland, K. 1989. Bistratified distribution of terminal arbors of individual axons projecting from area V1 to middle temporal area (MT) in the macaque monkey. *Visual Neurosci.* 3:155–170.

Schüz, A., and Münster, A. 1985. Synaptic density on the axonal tree of a pyramidal cell in the cortex of the mouse. *Neuroscience.* 15:33–39.

Segev, I., W. Fleshman, and R. E. Burke. 1989. Compartmental models of complex neurons. *In* Methods in Neuronal Modeling. From Synapses to Networks. C. Koch and I. Segev, editors. MIT Press. 63–93.

Segev, I. 1990. Computer study of presynaptic inhibition controlling the spread of action potentials into axonal terminals. *J. Neurophysiol.* 63:987–998.

Sereno, M. I., and P. S. Ulinski. 1987. Caudal topographic nucleus isthmi and the rostral nontopographic nucleus isthmi in the turtle, *Pseudemys scripta. J. Comp. Neurol.* 261:319–346.

Shepherd, G. M., and R. K. Brayton. 1979. Computer simulation of a dendro-dendritic synaptic circuit for self- and lateral-inhibition in the olfactory bulb. *Brain Res.* 175:377–382.

Stockbridge, N. 1989*a*. Theoretical response of a bifurcating axon with a locally altered axial resistivity. *J. Theor. Biol.* 137:339–354.

Stockbridge, N. 1989*b*. Solution of the Hodgkin-Huxley and cable equations on an array processor. *Ann. Biomed. Eng.* 17:253–268.

Stratford, K. J., A. U. Larkman, A. J. R. Mason, G. Major, and J. J. E. Jack. 1988. The modelling of pyramidal neurons in the visual cortex. *In* The Computing Neuron. R. Durbin, C. Miall, and G. Mitchison, editors. 296–321.

Swadlow, H. A., J. D. Kocsis, and S. G. Waxman. 1980. Modulation of impulses conduction along the axonal tree. *Ann. Rev. Biophys. Bioeng.* 9:143–179.

Traub, R. D., and R. K. S. Wong. 1983. Synchronized burse discharge in the disinhibited hippocampal slice. II. Model of the cellular mechanism. *J. Neurophysiol.* 49:459–471.

Waxman, S. G. 1975. Integrative properties and design principles of axons. *Int. Rev. Neurol.* 18:1–40.

Wilson, M. A., and J. M. Bower. 1989. The simulation of large scale neural network. *In* Methods in Neuronal Modeling. From Synapses to Networks. C. Koch and I. Segev, editors. MIT Press. 291–333.